Meccanica
DOI 10.1007/s11012-015-0241-x

SOFT MECHATRONICS

A rotary joint for a flapping wing actuated by dielectric elastomers: design and experiment

Jianwen Zhao · Junyang Niu · David McCoul · Jinsong Leng · Qibing Pei

Received: 1 October 2014 / Accepted: 2 July 2015

Abstract Exhibiting high energy densities, light weight, and elegant form factor, dielectric elastomers are poised as a promising alternative to the driving of flying robots. A rotary joint for a flapping wing actuated by a dielectric elastomer minimum energy actuation mechanism is reported. The deformation process and characteristics of the dielectric elastomer during joint rotation are analyzed, and the DE film will warp like saddle surface. The geometry parameter of the rotary joint will influence voltage-induced strain of DE film, and the natural frequency will restrict dynamics performance of the joint. Additionally, experimental results validate the characteristic of above saddle surface and the influence principle. A rotary joint and a flapping wing prototype were fabricated to validate design principles, demonstrating the design principles can be used to this kind of dielectric elastomer joint and flapping wing.

J. Zhao (✉) · J. Leng
Postdoctoral Research Station of Material Science and Engineering, Harbin Institute of Technology, Harbin 157401, China
e-mail: zhaojianwen@hit.edu.cn

J. Zhao · J. Niu
Department of Mechanical Engineering, Harbin Institute of Technology, Weihai 264209, China

J. Zhao · D. McCoul · Q. Pei
Department of Materials Science and Engineering, UCLA, Los Angeles, CA 90095, USA

Published online: 17 July 2015

Keywords Dielectric elastomer actuators (DEA) · Flapping wing · Artificial muscles · Dielectric elastomer minimum energy structures (DEMES)

1 Introduction

Humans have always dreamed of flying like birds in the sky. To realize the dream of flying, from the balloon to the airship to the aircraft, humans are ever advancing research in this field. Recently, the inception of the MAV [1] (micro air vehicle) has driven many new unmanned flight endeavors, including those for military applications, scientific investigation, and rescue and detection missions.

At present, the fixed wing [2], quad rotor [3], and flapping-wing [4] controlled MAVs are the most popular. From bionic and aerodynamic standpoints, the structure of the flapping-wing is arguably superior to the fixed wing and quad rotor designs when the size of the MAV is required to be as small as a bird or an insect. Namely, the flapping wing design presents the following key advantages:

1. Higher efficiency in generating lift. The effective propulsion of the flapping wing is up to 85 % higher than traditional propulsion systems [5, 6].
2. Integration of lift, hovering, and propulsion into one system. The control of an MAV's attitude can be rapid as a result of the motion of the flapping wing design.

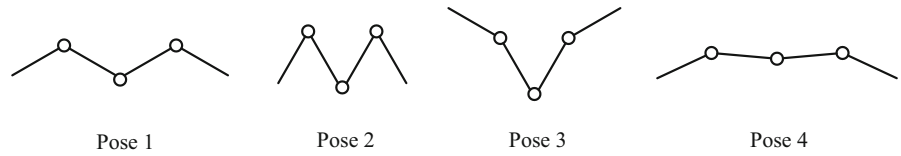

Fig. 1 The flapping motion of a bird can be simplified into four poses, each represented by a four-segment, three-joint structure

3. Energy conservation through the ability to glide. The flapping wing MAV can remain in a horizontal position and utilize potential energy to glide. Thus, more energy can be saved in comparison with the rotation of propeller.

Based on all the advantages above, the flapping-wing MAV is well suited for missions requiring long distance, low power flight.

The rotary joint of flapping-wing MAVs is similar to the joint between the wing and body of birds. Thus far, several MAV actuation modalities have been proposed, such as electromagnetic [7, 8], piezoelectric [9, 10], and EPAM (electroactive polymer artificial muscle) [11]. In the first driving modality, AeroVironment, Inc. have developed a flapping wing MAV "nano-humming bird" with 16 cm wingspan and 20 g weight In the second case [8], Harvard university have developed a piezoelectric flapping wing MAV with 3 cm wingspan and 60 mg weight [10]. This MAV utilizes a new micro-fabrication paradigm called Smart Composite Microstructures, enabling a flapping frequency of up to 110 Hz and a flapping angle greater than 50°.

As a new kind of actuator, dielectric elastomers (DEs) have attracted much attention [12–15]. DEs have demonstrated very high energy densities, seventy times higher than conventional electromagnetic actuators [16]. Low frequency actuation of DEs avoids the need for transmission gearing and allows for lighter weights of future robots. In addition, DEs have a lower cost than competing actuation technologies, positioning DEs as an economical alternative to powering MAV flight, and encouraging the use of swarm-MAVs [17]. In this paper, a new prototype of a rotary joint actuated by DEs is presented. The entire joint was efficiently designed using a dielectric elastomer minimum energy structure (DEMES) approach, recently proposed by Kofod et al. [18]. Such a rotary joint has higher torque to mass ratio, as well as larger angular displacement at high frequencies. The goal of this work is to provide more references toward the realization of flapping-wing MAVs actuated by dielectric elastomers.

2 Structure of the wing and the joint

The wing of a bird can be simplified into four segments with three joints. The lift force is generated through the coordination of the motion of all three joints as shown in Fig. 1.

To imitate the motion of a bird, three similar rotary joints were proposed to design the flapping wing. Using the DEMES approach, a light-weight wing system can be fabricated, capable of flexible, noiseless deformation. Each joint of the wing system was designed by balancing the torque between a pre-strained DE film and a flexible, semi-rigid frame. The restoring force of the DE film bends the elastic frame into a minimum energy state (Fig. 2). After applying kilovolts of low-current electricity on the dielectric

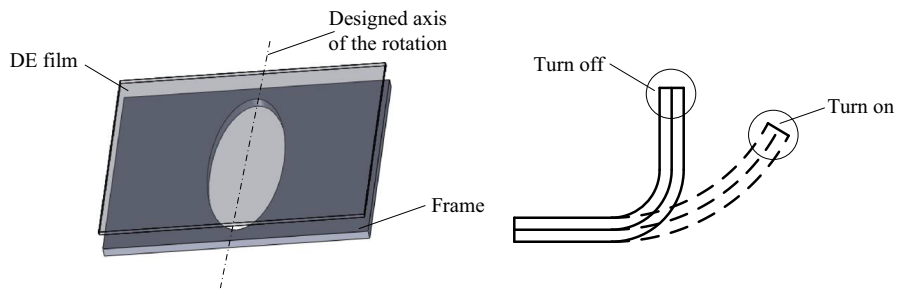

Fig. 2 Structure of the DEMES rotary joint

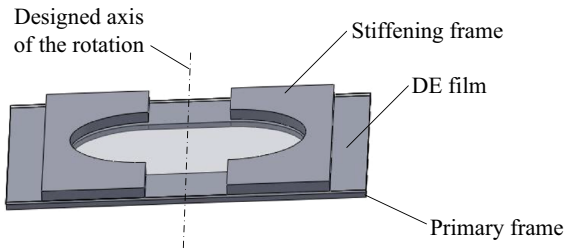

Fig. 3 The rotary joint with semicircular stiffening elements

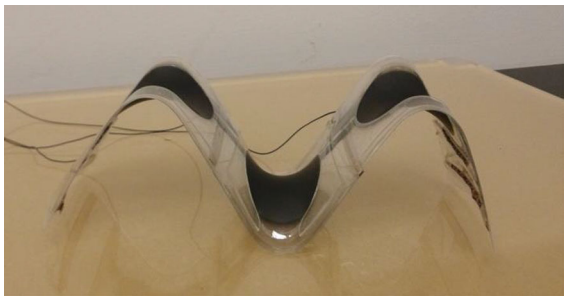

Fig. 4 Flapping wing system formed from joining three DEMES rotary joints together

elastomer, the frame flattens out, and the bending angle decreases. In this way, dynamically changing the voltage can dynamically and continuously alter the joint angle.

Further fabrication details are provided in Ref. [19]. To restrict frame bending to only one axis, the rigidity of the non-bending edges was enhanced by mounting two stiffening frames, as illustrated in Fig. 3.

The joint design shown in Fig. 3 was then expanded into the flapping wing system shown in Fig. 4.

3 Design principle of the joint

3.1 Static analysis of the DE film

For static analysis of the DE rotary joint, let us assign a fixed reference coordinate system such that the origin O is placed at the centroid of the elliptical area, as shown in Fig. 5a. The z-axis is shown in Fig. 5b.

The morphology of the DE film at the central elliptical hole of the frame is depicted in Fig. 6. The edge of the film is in a state of tensile stress F that creates a force component in z-direction, as shown in Fig. 5b. In turn, the film warps like saddle under the force component F_z.

It can be speculated from the saddle surface morphology that the surface gradient of points $M_{1–4}$ on boundary $ABCD$ is zero. Simplify the tension force on boundary M_1AM_4 to an equivalent composite force at point A and is named F_r. Similarly, the tension force on boundaries M_1BM_2, M_2CM_3, and M_3DM_4 are simplified to equivalent forces acting at points B, C, and D. By symmetry, the tension force at point A equals that at point C, and the force at B equals that at D. Force F_r has a positive component along the z-axis in the xz-plane. Force F_R has a negative component along the z-axis in the yz-plane. The magnitude of the component of F_r in the positive z-direction $F_{r–z}$ is greater than the magnitude of the component of F_R in the negative z-direction $F_{R–z}$ before the film has not been buckled, because $F_{R–z} = 0$. The result is causing the DE film to buckle upwards. The $F_{r–z}$ is decreasing while the $F_{R–z}$ is increasing with buckle upwards. The height of the film buckle is determined when $F_{r–z}$ and $F_{R–z}$ reach static equilibrium.

The component of F_r along z axis is decreasing while the component of F_R along z axis is increasing along with summon up of the film. The height of the film will summon up to a certain magnitude when the two components reach equilibrium.

3.2 Influence of parameter b to electrostrictive properties

The thickness of the DE film (VHB^{TM} 4910) is 40–50 μm after 400 % biaxial prestrain. Because the dimension of parameters a and b are at least 10 mm (approximate wing dimensions of a small bird), the thickness of the DE can be neglected when the static model is being established. The simplified DE film and frame in static equilibrium is shown in Fig. 7. Let h be the deviation of the DE film from the arc of the frame curvature and θ be the joint angle.

To analyze the influence of parameter b, two frames with same a value and different b values was taken as example and shown in Fig. 8. Without loss of generality, suppose $b_1 < b_2$.

Then, if we place the two frames onto the same coordinate system, they will assume the height protrusions h_1 and h_2 shown in Fig. 9. This is assuming that both DE films have the same prestrain ratios and frame thicknesses.

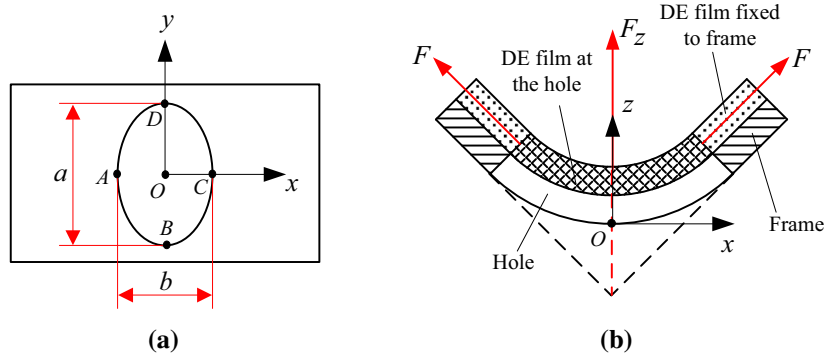

Fig. 5 Free body diagrams of the rotary joint. **a** Top view of the joint frame and the defined coordinate system. **b** Cross section of the joint frame, illustrating the forces acting on the DE film

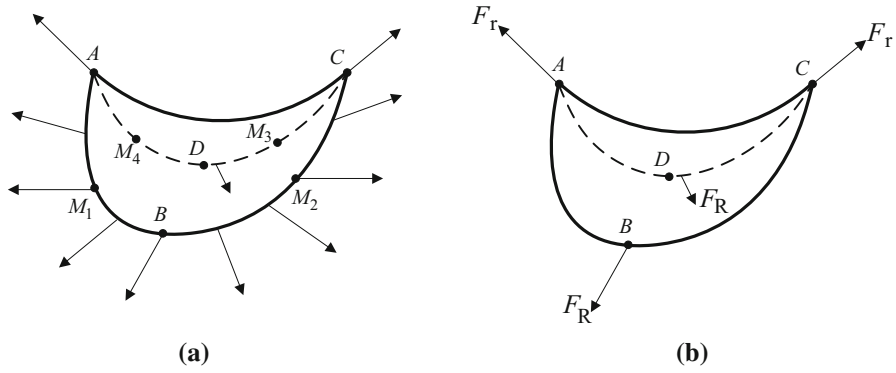

Fig. 6 Free body diagrams of the active DE saddle. **a** Representative forces at the edges of the DE film saddle. **b** Equivalent forces at select points

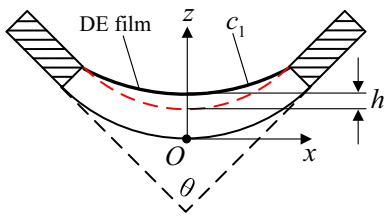

Fig. 7 Cross section of the DEMES joint in static equilibrium

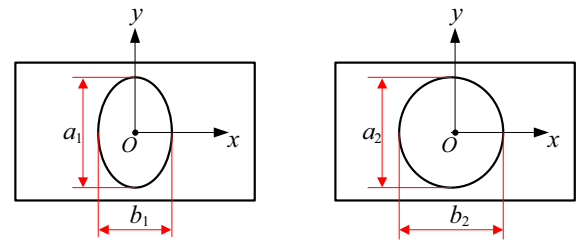

Fig. 8 Two frames with different parameter *b*

Let the arc lengths of Film 1 and Film 2 in Fig. 9 be l_1 and l_2. Let us define l/b to be the prestrain loss ratio, in which prestrain loss is minimized when l/b is as close to 1 as possible. Minimizing prestrain loss is of interest because more loss means decreased electromechanical performance. There is a transient state that makes the two crescent areas be geometrically similar, i.e., the same shape. Then we may write the geometric proportion $h_1/b_1 = h_2/b_2$, and therefore $l_1/b_1 = l_2/b_2$ for Films 1 and 2. Thus, since $b_1 < b_2$, it follows that $h_1 < h_2$. The length of a of the two frames are equal, so the flexure of Film 2 is larger than that of Film 1 in the yz-section shown in Fig. 10.

The length of Film 2 is longer that Film 1, so the strain and tension stress of Film 2 is larger. Since $b_2 > b_1$, $F_{R2} > F_{R1}$ (the definition of F_R is shown in Fig. 6). Since there is a larger extent of warp for Film 2 in the yz-plane (shown in Fig. 10), there is also a larger component of force in the z-direction generated by F_R in Film 2, i.e., $F_{R2\_z} > F_{R1\_z}$.

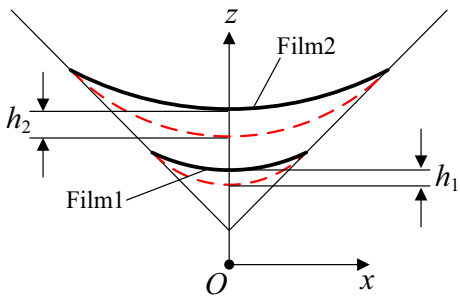

Fig. 9 DE film deflections resulting from increasing the frame hole width b_1 to b_2, keeping all other parameters fixed

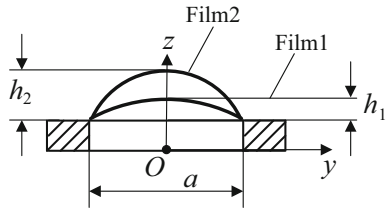

Fig. 10 Deflection of DE films in the *yz*-plane

When we assume $l_1/b_1 = l_2/b_2$, the boundary formed by l_1 and b_1 is the same shape as the boundary formed by l_2 and b_2, due to geometric similarity. Also, the two films have equal length a in the y-direction, so the component forces of the two films in the z-direction are equal as well, i.e., $F_{r1\_z} = F_{r2\_z}$. If the state of Film 2 in Fig. 9 is at equilibrium, i.e., $F_{r2\_z} = F_{R2\_z}$, then it can be deduced that $F_{r1\_z} > F_{R1\_z}$ by combining the above three expressions, namely: $F_{R2\_z} > F_{R1\_z}$, $F_{r1\_z} = F_{r2\_z}$, and $F_{r2\_z} = F_{R2\_z}$.

Therefore, the state of Film 1 shown in Fig. 9 is not stable, and Film 1 will continue to warp. More of the prestrain of Film 1 will be lost than the prestrain of Film 2 due to the increase of h_1 and the decrease of l_1/b_1. This behavior can also be explained by the law of energy conservation. The deformation energy is determined by the area of the film in the region bounded by the elliptical frame hole. The area of the hole in frame 1 is smaller than the area in frame 2, so the loss ratio of area and strain of Film 1 will be larger when providing the same deformation energy compared with Film 2. The value of l/b decreases with increasing swelling height h. The minimum value of l/b is $\sqrt{2}/2$ as the angular deformation reaches 90°. In this extreme state, the prestrain should be as high as 466 to ensure 300 % residual strain in the x-direction. But this prestrain ratio is not in commonly used since it is difficult to obtain. Thus, the residual strain in x-direction can be guaranteed by increasing the length of b as much as possible. Taking all the above into consideration, the double semicircle structure shown in Fig. 3 was experimentally tested in this paper.

3.3 Analysis of the natural frequency of the joint

During a single flapping stroke of the wing, the DE film is actuated once and the frame flattens out, and when the voltage is removed, the restoring force of the DE film returns the wing to its initial position. During multiple flapping events at a given frequency, the natural resonance frequency of the frame must not be less than the required frequency. Otherwise, the restoring response of the frame will limit the frequency required for lift since the recovery force is from the stored energy of the frame and his response can't faster than the response with natural frequency. Therefore, it is crucial to determine and fine-tune the natural frequency of the frame. For the discussion that follows, let us define the following frame parameters, illustrated in Fig. 11.

In the above figure, the thickness of the frame p, film, and stiffening member t is greatly exaggerated to show the structure more clearly. If we let the bending

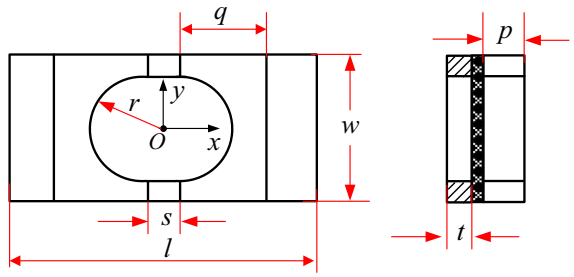

Fig. 11 Parameters of the joint frame. l total length, w total width, t thickness of primary frame (exaggerated), p thickness of stiffening frame (exaggerated), q width of each stiffening frame, s spacing between the stiffening frame, and r radius of each semicircle

Table 1 Parameters of the joint

E (GPa)	t (mm)	p (mm)	q (mm)	w (mm)	r (mm)	s (mm)	l (mm)
5.9	0.175	0.254	26	60	15	12.0	100

torque of the frame due to the DE film be T, then ignoring any rigidity of the DE film, the relationship between T and the joint angle θ is

$$T = \frac{E(w-2r)t^3}{12s}(\pi - \theta), \tag{1}$$

where E is the Young's modulus of the frame. Then, the natural frequency of the joint is given by

$$f = \frac{t}{2\pi}\sqrt{\frac{E(w-2r)t}{6Js}}, \tag{2}$$

where J is the rotary inertia of the frame along the y-axis. The inertia of the DE film was considered to be negligible. Moreover, the rotary inertia J can be calculated by the following expression:

$$J = \frac{1}{24}\rho twl^3 + \frac{1}{12}\rho qwp(4q^2 + 3s^2) - \frac{1}{12}\rho trs^3 - \frac{1}{8}\pi\rho r^2(t+p)(r^2+s^2) \tag{3}$$

With this mathematical model, we may adjust the natural frequency of the joint to be greater than the required lift frequency by changing the frame parameters.

Choosing plastic PET to make the frame and two layers of VHB4910, the parameters of the joint are shown in Table 1, with these parameters the natural frequency of the joint is 15.61 Hz that is satisfied to flapping wing (the flapping frequency of most birds is less than 10 Hz).

3.4 Design principle to optimize joint torque and weight

From Eq. (1), the flexural rigidity of the frame can be expressed as

$$K = \frac{E(w-2r)t^3}{12s} \tag{4}$$

For a DE film with 400 % × 400 % prestrain, it was experimentally demonstrated that an initial joint angle of 90° is most beneficial to the joint deformation under an electric field. Therefore, if the required joint torque is T_r, then the following expression should be satisfied:

$$K\frac{\pi}{2} > T_r \tag{5}$$

Then, to satisfy the natural frequency requirements, the rotary inertia can be altered by adjusting the frame parameters.

The joint consists of a thin frame, two stiffening frames, and some layers of DE films. Hence, if we let the area of the thin frame be S_1, the area of stiffening frame be S_2, and the mass of the DE film be M_{DE}, then the mass of the joint can be expressed as

$$M_{\text{Joint}} = \rho S_1 \sqrt[3]{\frac{12Ks}{E(w-2r)}} + 2\rho pS_2 + M_{\text{DE}}, \tag{6}$$

where ρ is the density of the frame material. From expression (5), the joint should have enough rigidity K to ensure that the joint can provide the required torque. With this requirement and by expression (6), to decrease the mass of the frame, the spacing between the stiffening frames s should be made as small as possible, fabrication permitting. Moreover, materials with ρ^3/E ratios that are as low as possible can also be

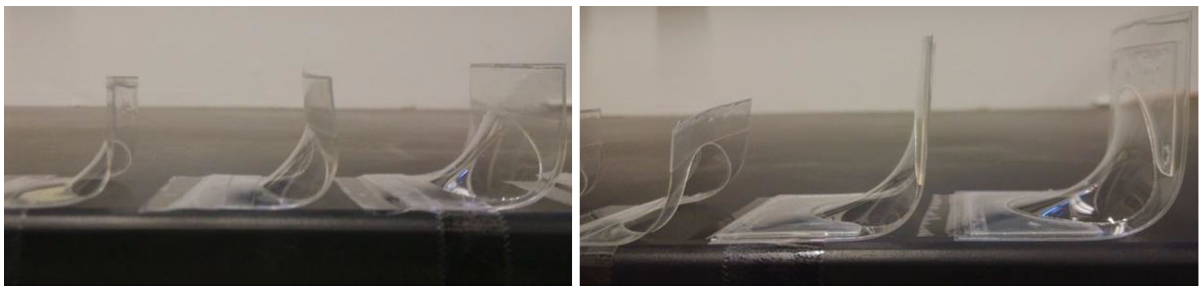

Fig. 12 DEMESs with $a = 35$ mm and $b = 15$, 20, 25, 30, 40, and 50 mm, from *left* to *right*

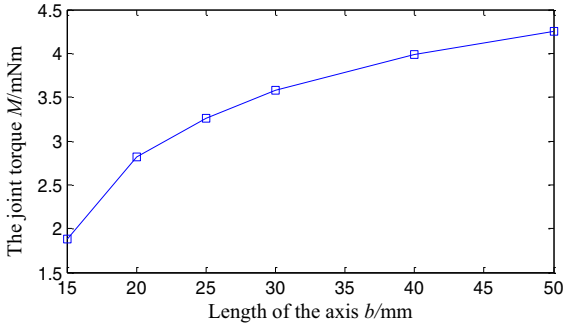

Fig. 13 The relationship between joint torque and dimension b

selected to increase the joint lightness. The values of p and S_2 are determined by the rigidity requirement in the y-direction, so these parameters can be optimized separately by desired the aerodynamic characteristics of the flapping wing.

4 Experiment

4.1 Fabrication

To prevent the electrode material from contaminating the frame, the electrodes were sprayed onto the DE film prior to adhering to the frame. Having chosen VHB^{TM} 4910 as the DE film and a biaxial prestrain of 400 % in each direction, the film can maintain a prestrain of at least 254 % at a joint angle of 90°. The primary and stiffening frames were made of laser-cut PET with a Young's modulus of 5.9 GPa. To improve contact between the semi-rigid frame and the soft DE films, the frames were cut at the appropriate laser power, and the frame edges were milled.

4.2 Experiment to validate the influence of hole width b to prestrain loss ratio

Keeping hole height a constant at 35 mm, DEMESs with the following b hole widths were fabricated: 15, 20, 25, 30, 40, and 50 mm, shown from left to right in Fig. 12. The joint angles shown are all about 90°, and a single layer of VHB^{TM} 4910 was utilized.

It can be found that the extent of warping of the DE film had decreased with increasing the of value b, that is, the prestrain loss ratio had decreased, thus validating the result of the theoretical analysis in Sect. 3.2.

The torque provided by the DE film on the above six joints with angle 90° is shown in Fig. 13. It can be seen that joint torque rises with increasing b, but the rate of this rise decreases gradually, approaching an asymptote.

4.3 Experimental validation of the influence of natural frequency on joint response driven at an alternating electric field

To validate the influence of natural frequency on the response of the joint, a joint demo was fabricated. An acrylic bar was mounted on the end of the frame to simulate load inertia. The laser sensor can detect

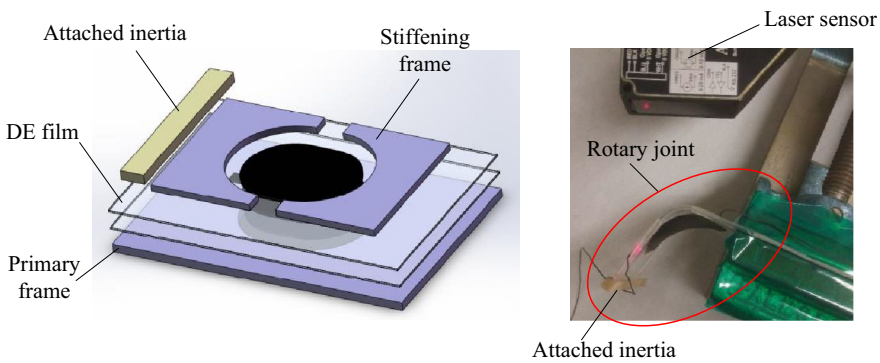

Fig. 14 Experiments to measure the actuation response of a DEMES rotary joint. The DE films consist of two layers of VHB^{TM} 4910 with 400 % biaxial pre-strain, the parameters are same as Table 1; the electrodes are carbon grease, and the laser displacement sensor is an Acuity AR200-50. **a** Structure of the rotary joint. **b** The system to measure the joint rotation

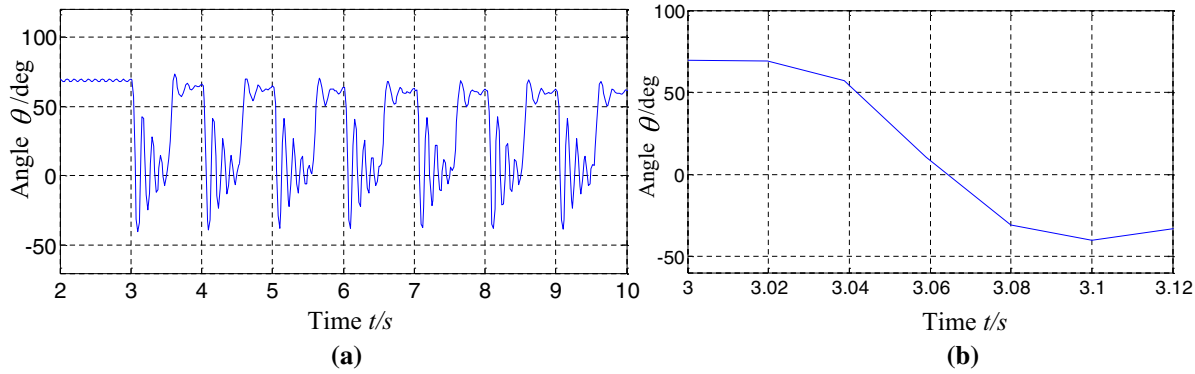

Fig. 15 Response of the joint driven with an alternating electric field 1 Hz; the voltage is a square wave with 5 kV amplitude and duty cycle ratio of 0.5. An acrylic bar with mass 1.2 g was affixed to the end of the joint. **a** The vibration with frequency 1 Hz. **b** The decay curve during free vibration

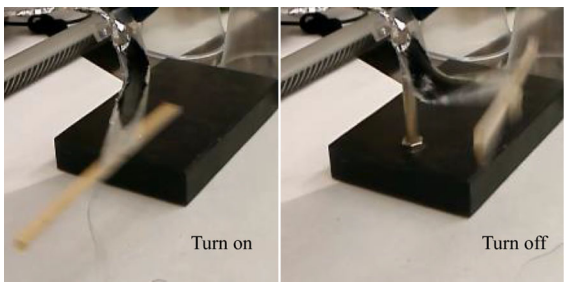

Fig. 16 Under the applied voltage of 5 kV and 3 Hz, gravity causes the joint to drive a larger inertia around the natural frequency, resulting in a joint angle of over 180°

angular displacement by method of Ref. [20] as shown in Fig. 14.

The natural frequency of the joint is about 6 Hz, which can be calculated by the decay curves of the joint rotation during free vibration, when the DE film was driven consistently at 5 kV. The vibration with 1 Hz alternating voltage is shown as Fig. 15a, and the decay curve are replotted from Fig. 15a with the scale enlarged as Fig. 15b.

The maximum frequency of the joint response is 6 Hz, other detailed information was described in Ref. [20]. The fastest response is restricted by natural frequency, so it is very important to increase the joint natural frequency. That validates the analysis results in part 3.3. The theoretical value of natural frequency calculated by Eq. (2) is 6.73 Hz that is greater than experimental result 6 Hz, the VHB film makes response of the joint slower.

4.4 Influence of gravity on deformability and load capacity of the joint driven with an alternating electric field

Letting the joint rotate about its horizontal axis, an acrylic bar of 6.2 g was mounted on the end of the frame as shown in Fig. 16. The mass of the joint is 1.2 g, and the natural frequency of joint with the acrylic bar is 3.35 Hz. Deformation of the joint at 3 Hz is shown. It was observed that gravity causes the joint angle θ to exceed 180°, resulting in resonance. This resonance makes the joint capable of driving a larger inertia of 155 g-cm^2. This resonance phenomenon could be used to further benefit the design of the flapping wing.

4.5 Experiment of a flapping wing composed by this DEMES joint

To validate if the DEMES joint can be used to compose a flapping wing, a prototype was fabricated. The middle joint was held to detect angular displacement of the joint. The vibration process with 5 Hz was recorded as follow

By a laser sensor as Fig. 14 and the method in Ref. [20] the angular displacements can be detected. All joints can realized over 60° with 5 Hz and are qualified for lifting of the wing, so the provided design principles are feasible to this kind of flapping wing. On power, as Fig. 17, with 5 Hz vibration, the average required power of this flapping wing is about 0.15 W.

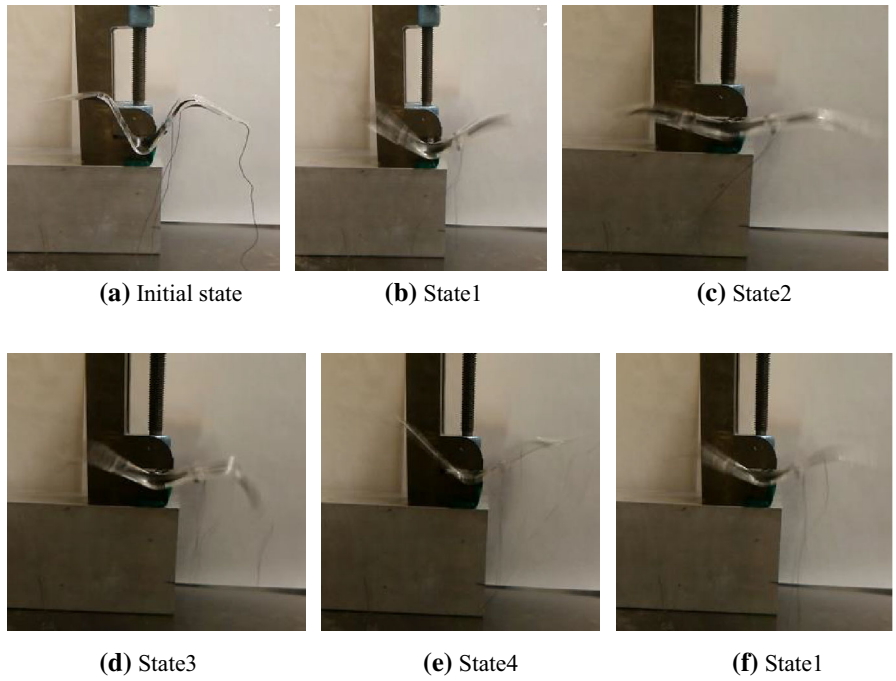

(a) Initial state **(b)** State1 **(c)** State2

(d) State3 **(e)** State4 **(f)** State1

Fig. 17 The vibration of the flapping wing with 5 Hz

After lifting, the vibration frequency will reduce greatly, so the required power will reduce too.

5 Conclusion

In the paper, we have presented the design, fabrication, and testing of a DEMES rotary joint to create flapping wing. The joint design is simplistic, consisting of only frame elements and a DE film. Based on statics analysis, natural frequency analysis, and experiment, the following design principles were obtained:

1. The shape of the DE film after joint deformation is a saddle surface, and the joint torque enlarges with increasing frame hole width b, although the extent of this enlargement reduces gradually. Additionally, the prestrain loss ratio decreases with increasing b, which is beneficial to the voltage-induced strain.
2. To improve the joint performance, i.e., to enable the joint to realize larger angular displacements under high frequency alternating electric fields, the mechanical natural resonance frequency of the joint should be made higher than the frequency of driving electric field.
3. Resonance makes the joint capable of supporting a larger inertia and realizing larger angular displacements. One of the necessary conditions for resonance is the ability of the joint to flex past $\theta = 180°$. Resonance may be incorporated into future designs by optimizing the inertia of the joint.

Using these principles, the joints of a flapping wing for DE-powered flight can be designed, fabricated, and optimized.

Acknowledgments This work was supported by National Natural Science Foundation of China (Grant No. 51205076), China Postdoctoral Science Foundation (Grant No. 2013M541359), Aerospace Foundation (Grant No. 2013-HT-HGD04) and China Scholarship Council.

References

1. Hundley RO, Gritton EC (1994) Future technology-driven revolutions in military operations. results of a workshop. RAND CORP SANTA MONICA CA Accession Number: ADA285478
2. Kim HJ, Kim M et al (2013) Fully autonomous vision-based net-recovery landing system for a fixed-wing UAV. Mechatron IEEE/ASME Trans 18(4):1320–1333

3. Pounds P, Mahony R, Corke P (2010) Modelling and control of a large quad rotor robot. Control Eng Pract 18(7):691–699
4. Liu H, Wang X, Nakata T, Yoshida K (2013) Aerodynamics and Flight Stability of Bio-inspired, Flapping-Wing Micro Air Vehicles. In: Autonomous control systems and vehicles, vol 65, Springer, Japan. pp 145–157
5. Betterid DS, Archer RD (1974) Study of mechanics of flapping wings. Aeronaut Q 25(MAY):129–142
6. Hall KC, Hall SR (1996) Minimum induced power requirements for flapping flight. J Fluid Mech 323(9):285–315
7. Ho S, Nassef H, Pornsinsirirak N et al (2003) Unsteady aerodynamics and flow control for flapping wing flyers. Prog Aerosp Sci 39(8):635–681
8. Keennon M, Klingebiel K, Won H, Andriukov A (2012) Development of the nano hummingbird: a tailless flapping wing micro air vehicle. In: AIAA aerospace sciences meeting, pp 1–24
9. Kevin Y, Ma PC, Sawyer B et al (2013) Controlled flight of a biologically inspired, insect scale robot. Science 340(6132):603–607
10. Wood RJ (2007) Liftoff of a 60 mg flapping-wing MAV. In: Intelligent robots and systems, 2007. IROS 2007, International conference on IEEE/RSJ. pp 1889–1894
11. Zdunich P, Bilyk D, MacMaster M et al (2007) Development and testing of the mentor flapping-wing micro air vehicle. J Aircr 44(5):1701–1711
12. Pelrine RE, Kornbluh RD, Joseph JP (1998) Electrostriction of polymer dielectrics with compliant electrodes as a means of actuation. Sens Actuators A Phys 64(1):77–85
13. Brochu P, Pei Q (2010) Advances in dielectric elastomers for actuators and artificial muscles. Macromol Rapid Commun 31(1):10–36
14. Giousouf M, Kovacs G (2013) Dielectric elastomer actuators used for pneumatic valve technology. Smart Mater Struct 22(10):104010
15. Zhao J, Niu J, Yu J (2014) A soft creeping robot actuated by dielectric elastomer[C]//SPIE smart structures and materials + nondestructive evaluation and health monitoring. In: International Society for Optics and Photonics. p 905608-905608-6
16. Andreas W, Matthew DL, Steven D (2006) On the design of large degree-of-freedom digital mechatronic devices based on bistable dielectric elastomer actuators. IEEE/ASME Trans Mechatron 11(4):448–456
17. Karpelson M, Wei GY, Wood RJ (2008, May) A review of actuation and power electronics options for flapping-wing robotic insects. In: Robotics and automation, ICRA 2008. IEEE International Conference on robotics and automation pp 779–786
18. Kofod G, Wirges W, Paajanen M, Bauer S (2007) Energy minimization for self-organized structure formation and actuation. Appl Phys Lett 90(8):081916
19. Kofod G, Paajanen M, Bauer S (2006) Self-organized minimum-energy structures for dielectric elastomer actuators. Appl Phys A 85(2):141–143
20. Zhao J, Niu J, McCoul D, Ren Z, Pei Q (2015) Phenomena of nonlinear oscillation and special resonance of a dielectric elastomer minimum energy structure rotary joint. Appl Phys Lett 106(13):133504